Journal of Magnetism and Magnetic Materials 474 (2019) 83–89

Contents lists available at ScienceDirect

Journal of Magnetism and Magnetic Materials

journal homepage: www.elsevier.com/locate/jmmm

Research articles

Magnetic properties of Ce doped M-type strontium hexaferrites synthesized by ceramic route

Khalid Mehmood Ur Rehman[a,1], Muhammad Riaz[b,1], Xiansong Liu[a,*], Muhammad Wasim Khan[a], Yujie Yang[c], Khalid Mujasam Batoo[d], Syed Farooq Adil[e], Mujeeb Khan[e]

[a] Engineering Technology Research Center of Magnetic Materials, School of Physics & Materials Science, Anhui University, Hefei 230601, PR China
[b] Department of Physics, University of the Punjab, Lahore 54590, Pakistan
[c] Computational Physics Key Laboratory of Sichuan Province, School of Physics and Electronic Engineering, Yibin University, Yibin 644007, PR China
[d] King Abdullah Institute for Nanotechnology, King Saudi University, P.O. Box 2455, Riyadh 1145, Saudi Arabia
[e] Department of Chemistry, College of Science, King Saud University, P.O. Box 2455, Riyadh 11451, Saudi Arabia

ARTICLE INFO

Keywords:
M-type hexaferrites (MHF)
Ce doping content
$Sr_{1-x}Ce_xFe_{12}O_{19}$ (SCFO)
X-ray diffraction (XRD)
Magnetic properties
Ceramic process

ABSTRACT

This paper highlights the experimental study of Ce^{3+} ions doped M-type hexaferrite $Sr_{1-x}Ce_xFe_{12}O_{19}$ ($0.00 \le x \le 0.30$) prepared by adopting the conventional ceramic process. The M-type hexagonal structure is confirmed in the X-ray diffraction measurements. There were two phases recognized for the magnetic powders with varying Ce content, one in-between $x = 0.00$ to 0.20 as a single magneto plumbite segment and the other at $x \ge 0.20$ as a second phase or the so called α-Fe_2O_3 phase. The micrographs of the sintered magnets depicted hexagonal crystal shapes. For magnetic properties a systematic study was done on the room temperature B–H hysteresis measurements. The estimated remanence value first increases with x in the range of $x = 0.00$ to 0.15 and then showed a decrease at $x \ge 0.15$. Besides, the intrinsic coercivity (H_{cj}) and magnetic induction coercivity (H_{cb}) show decreasing-increasing character while maximum energy product (BH_{max}) and ratio H_k/H_{cj} demonstrate increasing-decreasing character in the Ce doping range x of $x \le 0.15$ and $x > 0.15$ respectively.

1. Introduction

In last decade, strontium and barium hexagonal ferrites persist to attract the attention of researchers and scientists in various fields of science and technology [1–9]. The M-type hexagonal ferrites (MHF) fall in the category of magnetic materials (ceramic) and importantly participated in several hi-tech and manufacturing fields owing to their low cost, excellent chemical strength, great uniaxial magneto crystalline anisotropy and last but not the least simple production routes [10–12]. Besides, MHF have been widely applied in the form of permanent magnets, for instance information storage devices, loudspeakers, home appliances, and motors etc., to name a few [13]. In addition, recently there is a vast interest in MHF, as some of them belong to multiferroic materials even at room temperature and have large magneto-electric influence, which is associated with the presence of spinoidal and spiral magnetic structures [14–16]. In several MHF, where ferroelectric and ferromagnetic segments co-exist, one can control these segments by applying either an external electric field or magnetic field. Nevertheless, now a day's, M-type MHF attracts more attention as a multiferroic i.e. a materials that demonstrates a significant association between its magnetic and dielectric properties [17–19]. All the above materials used in spintronis, which is novel in the field of microelectronics [20–23]. However, at room temperature the ferroelectric state can be achieved by chemical substitutions or by magnificent local strains. Consequently, in solid solutions the concentration of d^5 cations in iron crystallographic positions decreases diamagnetically substituted and dipole-dipole ordering becomes possible at prominent temperatures. In electric field at 110 kV/m, Al-aggregation $BaFe_{12-x}Al_xO_{19}$ ($x \le 1.2$) hexaferrites the electric polarization of 0.6 μC/cm^2 and strong coupling between magnetic and electric subsystems at normal temperature were found [24,25]. Moreover, the diamagnetic replacement can basis a canted magnetic structure, which also prop ups the stabilization of the ferroelectric state [26,27]. In literature one can find MHF synthesized by several techniques, including sol-gel and sol-gel auto combustion [13,14], citrate precursor process [15,16], Pechini process [28], solution combustion route [29], modified chemical coprecipitation method [30] hydrothermal method [2,3,31,32] and the ceramic process [12,33]. Among all above routes the ceramic method is

* Corresponding author.
E-mail address: xiansongliu@ahu.edu.cn (X. Liu).
[1] Both authors KMUR and MR contributed equally to this work.

https://doi.org/10.1016/j.jmmm.2018.10.087
Received 9 March 2018; Received in revised form 20 September 2018; Accepted 17 October 2018
Available online 19 October 2018
0304-8853/

frequently used to prepare magnetic oxides which require multiple annealing and sintering steps [34]. It is important to recall that in MHF type structure, Fe^{3+} ions utilize five opposing sites, i.e., three spin up sites (2a, 2b and 12 k) and two spins down sites ($4f_1$ and $4f_2$). Here 2a, 12 k and $4f_2$ are octahedral sites, $4f_1$ is tetrahedral site and 2b is bi-pyramidal site [35]. Furthermore, the magnetic moment as well as magneto-crystalline structure appear from the electronic anisotropy of Fe^{3+} ions at the above five opposing sites [36]. In order to fulfill various needs in magnetic storing devices, many cations (La^{3+}, Pr^{3+}, Sm^{3+}, Nd^{3+}, Co^{2+}, Ti^{4+}, Mn^{2+} etc.,) and cations combinations (La^{3+}-Co^{2+}, La^{3+}-Zn^{2+}, La^{3+}-Cu^{2+}, La^{3+}-Bi^{3+} etc.,) have been tried. A survey of literature for high density perpendicular recording media suggest that in La^{3+} substituted strontium hexaferrite nanoparticles prepared by citrate precursor method show increase in coercivity value by increasing La^{3+} composition and has high value at $x = 0.63$ [37–40]. Recently, structural and magnetic properties of M type Ce substituted barium hexaferrites prepared by Sol–gel auto combination method were studied [13]. Microwave absorption properties of Ce-substituted barium ferrite prepared by the citrate sol–gel method were also investigated recently [15]. A study regarding improvement in the magnetic properties of strontium hexaferrite via Al doping is discussed very recently by Wang et al. [41]. Effect on structural and magnetic properties due to replacement of Sr^{2+} ions by rare-earth ions (RE^{3+}) ions (RE: Y, La, Ce, Pr, Nd, Sm, and Gd) have been investigated for the case of Sr ferrites [42]. A systematic study on structural and magnetic properties of M-type strontium hexaferrite particles, prepared by a modified chemical coprecipitation method is done by Zi et al. [30]. There are also reports about the compound $Sr_{1-x}La_xFe_{12-x}Cu_xO_{19}$ in the doping range of ($0.0 \le x \le 0.35$) prepared via the standard ceramic route revealed that the coercivity decease linearly by increasing x (i.e., $0.0 \le x \le 0.35$) just like work of Yang et al. [43,44]. The strontium based MHF containing La^{3+} and Bi^{3+} with the formula $Sr_{1-x}La_xFe_{12-x}Bi_xO_{19}$ ($0.0 \le x \le 0.5$) prepared by sol-gel auto combustion technique have also been studied in recent times [45]. Moreover, study of Co-Zr substituted strontium hexagonal ferrites $SrCo_xZr_xFe_{12-x}O_{19}$ with ($0.0 \le x \le 1.0$) produced by sol-gel process also showed some intriguing properties [46–48]. The presence of magnetically ordered states and ferroelectric properties open new opportunity for wide practical application of the MHF. The key point for such applications is controlling the magnetic properties of such specimens. The analysis of experimental data of multicomponent oxides so as the hexaferrites confirmed that their physical properties are directly depended on concentration of diamagnetic substitute, type of crystal structure, crystalline size [27] and even confirmed the anion stoichiometry [25]. In this paper we expose the study of Ce^{3+} ions doped Sr based MHF having following formula $Sr_{1-x}Ce_xO.6Fe_2O_3$ or $Sr_{1-x}Ce_xFe_{12}O_{19}$ (from here onward we will call it SCFO) in the form of powders and magnets, within the doping range $0.00 \le x \le 0.30$ prepared by the conventional solid state ceramic process. The main aim behind this work is to probe composition effects of Ce^{3+} ions on the magnetic and microstructure related properties of SCFO magnets.

2. Materials and methods

2.1. Materials

We highlight that seven samples of MHF doped with Ce^{3+} ions having following formula $Sr_{1-x}Ce_xFe_{12}O_{19}$ (SCFO) with $0.00 \le x \le 0.30$, were prepared in succession by the standard ceramic process by choosing raw materials of AR grades namely $SrCO_3$ (99 wt %), Ce_2O_3 (99 wt%) and Fe_2O_3 (98 wt%).

2.2. Methods

In order to achieve required mixtures, a planetary ball mill was used with hardened steel balls containing 10 mm average diameter and having a speed of 310 rpm. Briefly, as a first step, mixed powders prepared by the wet mixing method presintered in air, inside a box furnace at about 1280 °C for 2 h. A vibration mill was used to crush down the particles less than 100 μm, and then sent to a ball mill where they wet milled with appropriate additives (0.5% wt. of $CaCO_3$, 0.3% wt. of SiO_2, 0.2% wt. of Al_2O_3 and 0.3% wt. of H_3BO_3) for about 14 h. This final milled product was trampled into disc-shaped pellets having roughly 15 mm thickness and 30 mm diameter under 310 MPa in a pulsed magnetic field aligned parallel to the pressing direction and having value of 900 KA/m. For the second step, the green compacts were sintered again in air at the temperature 1220 °C for 1.5 h inside the box furnace. The structural information regarding phase components of the presintered powder samples were carried out by an analytical difractometer (X'Pert Pro) in continuous mode using Cu Kα radiation having λ = 1.5406 Å. In order to investigate morphologies, a field emission scanning electron microscopy FE-SEM (HITACHI S-4800) was used. Magnetic properties were carried out at room temperature by using a permanent magnetic measuring system (NIM-2000HF, made by the National Institute of Metrology of China).

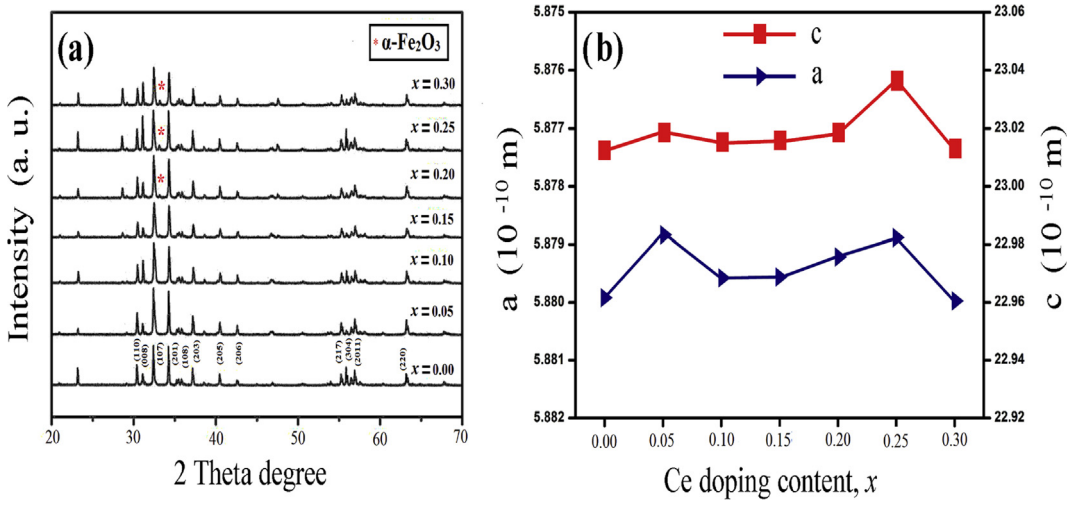

Fig. 1. (a) XRD pattern for the MHF powders of SCFO ($0.00 \le x \le 0.30$), (b) Plot of lattice parameters a and c versus x of SCFO ($0.00 \le x \le 0.30$).

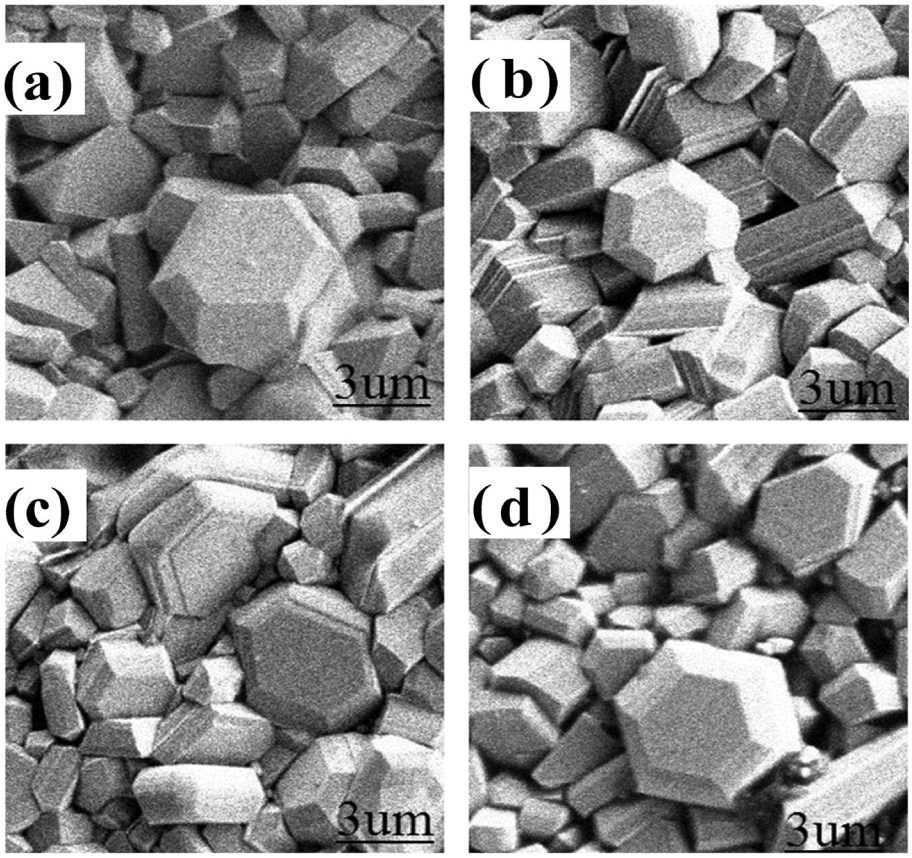

Fig. 2. FE-SEM images of the SCFO ($0.00 \leq x \leq 0.30$) magnets sintered at 1220 °C for 1.5 h (in air) with Ce composition (x) of; (a) $x = 0.00$, (b) $x = 0.05$, (c) $x = 0.10$, and (d) $x = 0.15$.

3. Results and discussion

3.1. Phase identification analysis

The structural analysis of MHF powders of SCFO ($0.00 \leq x \leq 0.30$) acquired by X-ray diffraction (XRD) measurements is depicted in Fig. 1. The diffraction peaks are indexed by reason of hexagonal magneto plumbite crystal anisotropy having space group $P6_3/mmc$ (JCPDS card no.33-1340).

It is evident from Fig. 1(a) that all precursors have almost same XRD pattern that point toward a single magneto plumbite structure and no secondary phase's sign is seen with the increase of Ce doping content x from 0.00 to 0.15 due to entering various cations in the crystal structure of hexaferrites. This suggests that Ce^{3+} ions have gone into the M-type lattice. With $x \geq 0.20$, the XRD patterns show a desired phase of the strontium MHF and also an undesired phase or roughly speaking as a second hematite phase in the form of α-Fe_2O_3 with space group (R-3c). The occurrence of this sort of phase at $x \geq 0.20$, suggests that not all Ce^{3+} ions have entered in the MHF lattice of SCFO. In addition, it is evident that the peak intensities of XRD patterns changes by increasing x. The variation could be thought as due to occupying of the crystallographic sites in the crystal lattice. The strongest peak corresponds to (1 0 7), for the SCFO magnetic powders with x range of 0.00–0.30. In Fig. 1(b) we present results for the variant of the lattice constants a and c with different Ce doping content (x) for the powders of SCFO ($0.00 \leq x \leq 0.30$). These values of lattice constants a and c as a function of x are estimated from the values of the interplanar distances d_{hkl} given by the following formula,

$$d_{hkl} = \left(\frac{4}{3}.\frac{h^2 + hk + k^2}{a^2} + \frac{l^2}{c^2}\right)^{-\frac{1}{2}} \quad (1)$$

where h, k and l are the Miller indices and d_{hkl} is the inter-planer spacing.

As already mentioned, the obtained values for the respective lattice constants a and c are plotted in Fig. 1(b), show variation with the increase of Ce content (x). Fig. 1(b) shows that the values of lattice parameters c and a increase with increasing Ce^{3+} aggregation x for the powders of SCFO ($0.00 \leq x \leq 0.30$). The increase in lattice parameters c and a is ascending from the point that the average ionic radii (1.26 Å) of Sr^{2+} and (1.143 Å) of Ce^{3+} are higher as equated to the ionic radius (0.78 Å) of Fe^{3+}. The variation of c/a (lattice parameter ratios) as a meaning of Ce^{3+} aggregation x for the MHF is confirmed in Fig. 3. It is obvious from Table 1 and Fig. 3 that ratios of c/a are slightly increasing with the increasing of (x) aggregation of Ce^{3+} from 0.00 to 0.30. The c/a is exploited to confirm the structure type i.e for MHF structure can be assumed if the ratio is lower than 3.98. The c/a ratios are within the range of 3.910–3.916, specifying the MHF structure. It is obvious from Table 1 that with the variation of Ce^{3+}, x aggregation the unit cell volume (V_{cell}) increases from x aggregation 0.00–0.30 and 686.026$(A^0)^3$ to 692.096$(A^0)^3$. The increase of V_{cell} with increasing Ce^{3+} x-aggregation may be ascribed to the lattice parameters (c and a) as shown in Table 1 and Fig. 3. Furthermore, the change in the lattice constant c is bigger in comparison with lattice constant a. It is quite evident that both parameters show more or less a similar trend with increasing x i.e., an increase-decrease region followed by a constant type region and then again an increase-decrease region. It is well established now that the lattice constants should increase if one substitutes higher ionic radii elements [40]. The refined values of lattice parameters of crystal structure with space group $P6_3/mmc$ are listed in Table 1. The indexing and refinement of lattice parameters are confirmed by using software Checkcell (upgraded version of Celref) by using the least square method. The calculated crystallographic

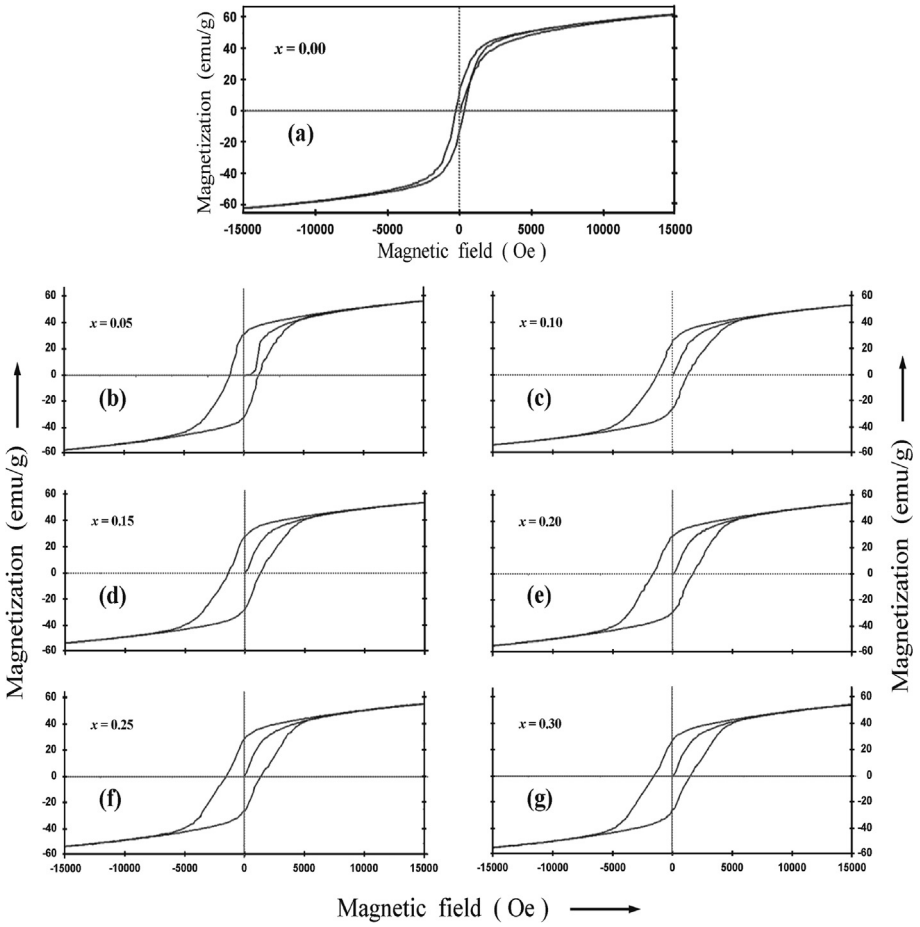

Fig. 3. Magnetization versus applied magnetic field of SCFO hexaferrite; (a)–(f) with different Ce doping content values ($0.00 \leq x \leq 0.30$).

Table 1
Parameters from the structural refinement of $Sr_{1-x}Ce_xFe_{12}O_{19}$ (x = 0.00, 0.05, 0.10, 0.15, 0.20, 0.25, 0.30).

Lattice Parameters	x = 0.00	x = 0.05	x = 0.10	x = 0.15	x = 0.15	x = 0.25	x = 0.30
a = b	5.8780	5.8804	5.8850	5.8879	5.8897	5.8901	5.8909
c (A^0)	22.9879	23.0071	23.0136	23.0372	23.0536	23.0680	23.0696
c/a	3.910	3.912	3.910	3.912	3.914	3.916	3.916
$\alpha = \beta(\theta^0)$	90	90	90	90	90	90	90
Υ (θ ^{0})	120	120	120	120	120	120	120
Volume $(A^0)^3$	686.026	687.845	688.962	689.478	690.471	691.718	692.096

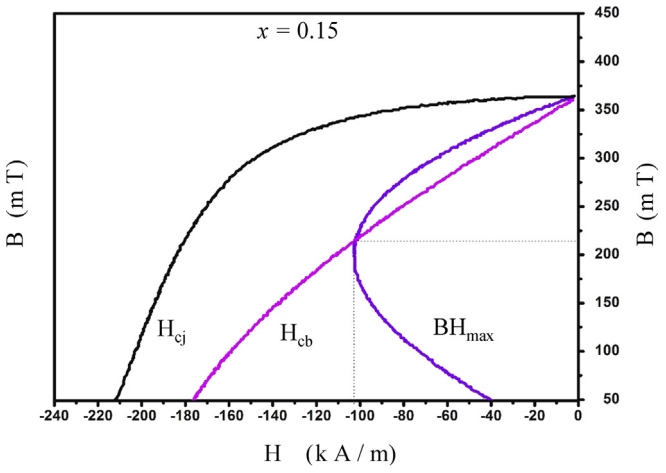

Fig. 4. The usual Demagnetizing curves of MHF magnets SCFO with Ce content x, at x = 0.15.

parameters show an increase and variations in lattice parameters with doping of Ce^{3+} ions which leads to the change in volume of doped sample.

We describe the SEM micrographs of the SCFO powders in Fig. 2((a)–(d)), in order to give an evident visualization about the homogeneous distribution and hexagonal plate like shape of the particles. In addition, it is observed that the Ce composition (x) do not affect the average particle size and precursor morphology of the sintered magnets.

3.2. Magnetic properties

The magnetic properties of MHF in the form of hysteresis loops for SCFO magnetic powders with different Ce doping content, x ($0.00 \leq x \leq 0.30$) are shown in Figs. 3 and 4 respectively. The demagnetizing curves (Fig. 3) of sintered magnets were recorded at room temperature for all the precursors by resorting to a permanent magnetic measuring system.

In Fig. 4 below, we describe a quick view of the typical

Table 2
Summary of B_r, H_{cb}, H_{cj} and $(BH)_{max}$ values taken from the data of MHF magnets SCFO with different Ce contents, x ($0.00 \le x \le 0.30$).

Ce content, x	B_r (mT)	H_{cb} (KA/m)	H_{ej} (ka/m)	$(BH)_{max}$(kJ/m^3)
0.00	246	161.3	1710	5.37
0.05	267	150.9	272	12.2
0.10	309	85.9	1131	15.9
0.15	324	61.4	1206	18.0
0.20	226	67.4	1349	5.10
0.25	224	74.3	1574	3.82
0.30	150	170.6	1580	2.85

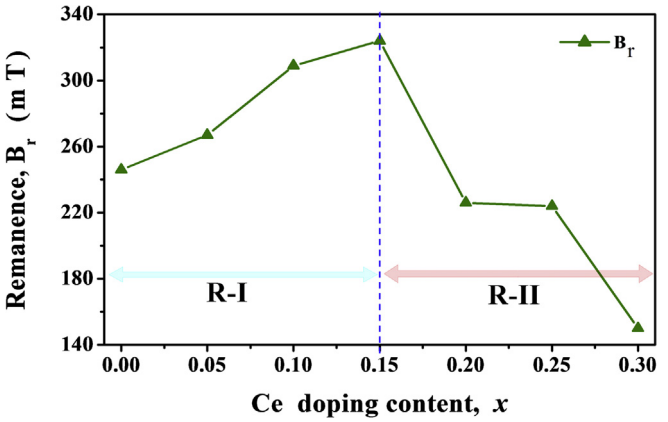

Fig. 5. The remanence (B_r) versus Ce doping content (x) plotted for the SCFO hexaferrites.

demagnetizing curves of SCFO magnets with constant value of Ce content $x = 0.15$.

Furthermore, the parameters determined from the obtained hysteresis loops for instance, the remanence (B_r), intrinsic coercivity (H_{cj}), magnetic induction coercivity (H_{cb}) and maximum energy product ($(BH)_{max}$) respectively are presented in Table 2.

In Fig. 5, we present data of SCFO hexaferrites in the form of remanence (B_r) with varying Ce doping content (x) in the range of ($0.00 \le x \le 0.30$). The B_r show fairly significant deviation such that initially it increases in the region marked as R-I at $x = 0.00$ (with B_r value ~246 mT) to $x = 0.15$ (B_r value ~324 mT). After that it showed a decrease when $x \ge 0.15$ (with B_r value ~324 mT to 150 mT) marked as region R-II. In our view, the increasing trend in Br value in the region R-I ($0.0 \le x \le 0.15$) is ascribed to occupancy of different interstitial sites by the Fe^{3+} ions (as discussed in sec. 1) together with collinear arrangement of its magnetic moments created by super exchange mechanism. Additionally, Ce^{3+} ions tend to reside on those sites that contain downward electrons spins in the low doping range, therefore the Fe^{3+} ions have to forcing upward spins and accordingly increasing the remanence. Alternatively, in $Sr_{1-x}Ce_xFe_{12}O_{19}$ ($0.00 \le x \le 0.30$), the replacement of trivalent of Ce^{3+} for divalent Sr^{2+} ions a small quantity of Fe^{3+} ions will change into Fe^{2+} ions at octahedral 2a sites to balance the electric charge. This decline the ferromagnetic Fe^{3+}–O^{2-}–Fe^{3+} super exchange interaction due to valence change [46,47]. Consequently, strong local spin-canting exist the overall magnetic structure remains ferrimagnetic up to $x \ge 0.20$. The results were gradual decrease in T_C by increase in Ce^{3+} substitution leads to the formation of a spin-canting structure [40,48]. Now let us shed some light on the shrinking of remanence (B_r) in the region R-II with $x > 0.15$. The increase in doping content of Ce^{3+} ions together with regards to its non-magnetic character will tend to reduce the already present super exchange effect and hence the B_r value. Furthermore, in above Ce substitution range R-II (i.e., $x > 0.15$) the α-Fe_2O_3 phase (as a second phase) will start to show up growing character in its composition with respect to increment in x and consequently become a cause of further decreasing the B_r value. Fig. 6(a) describes the dual variation of the magnetic induction coercivity (H_{cb}) together with the intrinsic coercivity (H_{cj}) as a function of Ce doping content (x).

First of all, clearly, observed that both H_{cb} and H_{cj} of the SCFO hexaferrites show a rapid decrease with increase in x values represented by R-I and R-II respectively. The H_{cb} decreases at $x = 0.00$ (having H_{cb} value ~161.3 KA/m) to $x = 0.15$ (with H_{cb} value ~61.4 KA/m). Then it showed an increase from $x = 0.15$ onwards (H_{cb} value ~61.4 KA/m) to $x = 0.30$ (having H_{cb} value ~170.6 KA/m). Similarly to above, the H_{cj} decreases at $x = 0.00$ (H_{cj} value ~1710 KA/m) to $x = 0.05$ (having H_{cj} value ~272 KA/m). After that it increases and showed almost a linear increasing character from $x = 0.10$ (H_{cj} value ~1131 KA/m) to $x = 0.30$ (having H_{cj} value ~1580 KA/m). In literature [49] one can find a theoretical formula relating inversely the coercivity (H_{cj}) with the saturation magnetization (M_S) given as under,

$$H_c = a\left(\frac{2K}{M_s}\right) \quad (1)$$

where a, M_S and K are called, the orientation factor, saturation magnetization and magneto crystalline anisotropy constant respectively. The decease of H_{cb} ($x < 0.15$) and H_{cj} ($x < 0.05$) may be seen from Eq. (1) and from Fig. 6(b) where B_r and H_{cj} are plotted together as a function of x. Besides, the increase of both H_{cb} and H_{cj} in the R-II having doping range $x \ge 0.15$ might be ascribed to the slight decrease seen in the B_r value in the vicinity of above mentioned range (see Fig. 6(b)). Lastly, there may be an influence of magneto crystalline anisotropy in

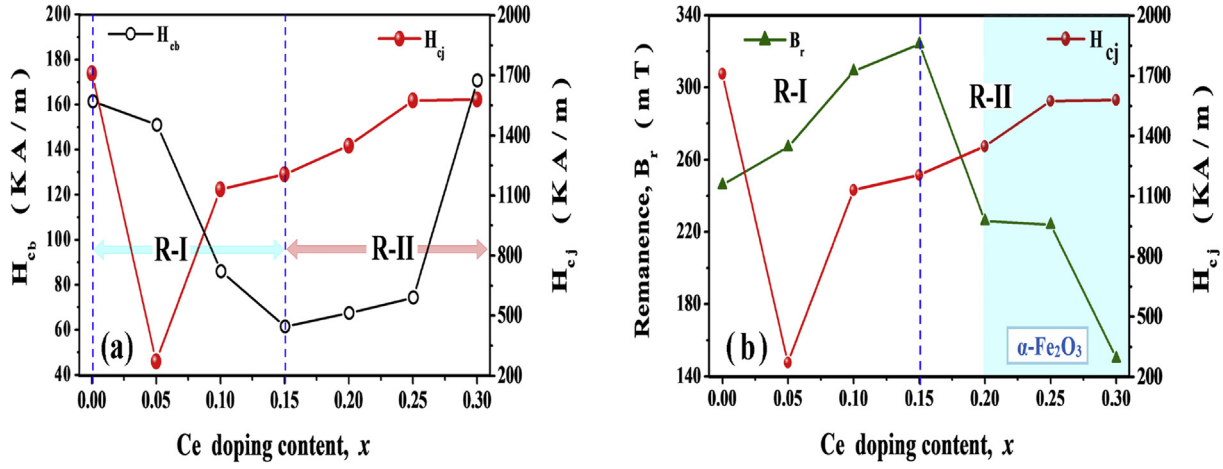

Fig. 6. The plot of H_{cb} (left vertical axis) and H_{cj} (right vertical axis) versus Ce doping content x, for the SCFO hexaferrites. R-I and R-II are regions of investigation.

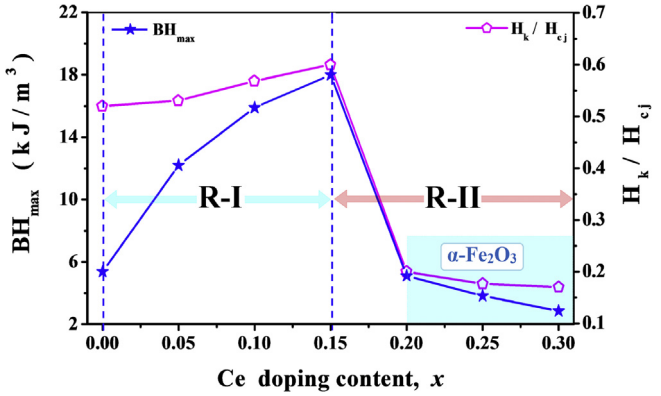

Fig. 7. BH_{max} and H_k/H_{cj} versus Ce doping content x, plotted on a dual vertical axis for the SCFO hexaferrites. R-I and R-II are two regions under investigation.

increasing the above parameters (H_{cb} and H_{cj}).

The plot of maximum energy product (BH_{max}) versus different Ce compositions x is shown in Fig. 7. First consider the left side axis of BH_{max} value, that show an increasing trend in the region R-I with $0.00 \leq x \leq 0.15$, while there is a decrease in its value in the region R-II ($x \geq 0.15$). Looking at Figs. 5 and 6 and also from the information given in Table 1, it is clear that the BH_{max} has shown a decreasing trend in R-II region at $x = 0.15$ (with $BH_{max} \sim 18.0\,kJ/m^3$) to $x = 0.30$ (having $BH_{max} \sim 2.85\,kJ/m^3$). This can be attributed to the variations of the remanence (B_r) and intrinsic coercivity (H_{cj}) as depicted in Fig. 6. It is well accepted that the BH_{max} is predictable by the product of B_r and H_{cj}, and is judged as maximum area (in the second quadrant) of the hysteresis loop. Therefore, above discussion confirmed that, the BH_{max} has shown a decrease with respect to increase in Ce doping x for the case of SCFO.Now let us turn to the right hand side axis of above Fig. 7, where the H_k/H_{cj} ratio of the SCFO ($0.00 \leq x \leq 0.30$) magnets as a function of x is presented. Here H_k and H_{cj} are the knee field and coercivity respectively. Actually, H_k/H_{cj} is a considered as a vital ratio in regard to magnetic properties of the permanent magnets. It can, by instinct, index the rectangularity of the demagnetizing curves as well as validate the stability of the magnets under dynamic working environment [50]. As seen from Fig. 7, in region R-I, the H_k/H_{cj} ratio has shown an increase similar to BH_{max} with increasing Ce content and in the region R-II it has shown a decrease in its value. The observed character of H_k/H_{cj} ration is accordance with the results revealed in Figs. 3 and 4.

4. Conclusion

The M-type hexaferrites (MHF) doped with Ce^{3+} ions having the general formula $Sr_{1-x}Ce_xFe_{12}O_{19}$ (SCFO) with $0.00 \leq x \leq 0.30$, were successfully prepared in succession by the standard ceramic process. XRD data confirmed the phase compositions of the powder samples by highlighting two phases, first as a single magneto plumbite phase with increasing x upto $x \leq 0.20$, and second as α-Fe_2O_3 when $x \geq 0.20$. The microstructures also confirmed that the grain particles were of hexagonal platelet like shape. For investigation of magnetic properties, a permanent magnetic measuring machine was used to record the measurements at room temperature. The estimated remanence value (B_r), showed an increases with x upto $x = 0.15$ and then a decrease when $x \geq 0.15$. The other parameters like intrinsic coercivity (H_{cj}) and magnetic induction coercivity (H_{cb}) showed a decreasing-increasing trend in the above regions of Ce doping. However, the maximum energy product (BH_{max}) and ratio H_k/H_{cj} have displayed increasing–decreasing character in the regions of $x \leq 0.15$ and $x > 0.15$ respectively with respect to increasing Ce doping content. Finally, the MHF with Ce doping (like SCFO) with $x \leq 0.15$ having high B_r and low H_c values, are of great interest for the future magnetic applications.

Acknowledgments

Both KMUR and MR contributed equally in preparing and drafting the manuscript. The following authors KMUR, X. L, Y. Y acknowledge the financial support from the National Natural Science Foundation of China under Grant Nos. 51272003 and 51472004. However, MR acknowledges financial support from grant 2013-14 by Punjab University Lahore, Pakistan. Author K.M. Batoo is thankful to the Deanship of Scientific Research at King Saud University for its funding through the Research Group Project No. RG-1437-030.

References

[1] J.P. Jakubovics, Magnetism and Magnetic Materials, 1st Ed., The Institute of Metals, London, 1987.
[2] J.F. Wanga, C.B. Pontonb, I.R. Harrisa, J. Magn. Magn. Mater. 234 (2001) 233–240.
[3] J.F. Wang, C.B. Ponton, R. Grössinger, I.R. Harris, J. Alloy. Compd. 369 (2004) 170–177.
[4] M.N. Akhtar, A.B. Sulong, M. Ahmad, M.A. Khan, A. Ali, M.U. Islam, J. Alloy. Compd. 660 (2016) 486–495.
[5] S.V. Trukhanov, A.V. Trukhanov, V.G. Kostishin, L.V. Panina, I.S. Kazakevich, V.A. Turchenko, V.V. Kochervinskiy, JETP Lett. 103 (2016) 100–105.
[6] K.M.U. Rehman, X. Liu, Y. Yang, et al., J. Magn. Magn. Mater. 449 (2018) 360–365.
[7] S.V. Trukhanov, A.V. Trukhanov, et al., J. Magn. Magn. Mater. 426 (2017) 487–496.
[8] S.V. Trukhanov, A.V. Trukhanov, V.A. Turchenko, V. An, E.L. Trukhanov, D.I. Trukhanova, V.M. Tishkevich, T.I. Ivanov, M. Zubar, V.G. Salem, L.V. Kostishyn, D.A. Panina, S.A. Gudkova, Vinnik, Ceram. Int. 44 (2018) 290–300.
[9] S.V. Trukhanov, A.V. Trukhanov, V.A. Turchenko, V. An, D.I. Trukhanov, E.L. Tishkevich, T.I. Trukhanova, D.V. Zubar, V.G. Karpinsky, L.V. Kostishyn, D.A. Panina, S.A. Vinnik, E.A. Gudkova, P. Trofimov, A. Thakur, Y. Yang Thakur, J. Magn. Magn. Mater. 457 (2018) 83–96.
[10] S.-W. Cheong, M. Mostovoy, Nat. Mater 6 (2007) 13.
[11] M. Gich, I. Fina, A. Morelli, F. Sánchez, M. Alexe, J. Gàzquez, J. Fontcuberta, A. Roig, Adv. Mater. 26 (2014) 4645.
[12] Y.J. Yang, X.S. Liu, D.L. Jin, Y.Q. Ma, J. Magn. Magn. Mater. 364 (2014) 11–17.
[13] R.A. Pawar, S.S. Desai, Q.Y. Tamboli, Sagar E. Shirsath, S.M. Patange, J. Magn. Magn. Mater. 378 (2015) 59–63.
[14] V.P. Singh, G. Kumar, A. Kumar, R.S. Rai, M.A. Valente, K.M. Batoo, R.K. Kotnala, M. Singh, Ceram. Int. 42 (2016) 5011–5017.
[15] Sun Chang, Sun Kangning, Chui Pengfei, J. Magn. Magn. Mater. 324 (2012) 802–805.
[16] K. Rana, P. Thakur, A. Thakur, M. Tomar, V. Gupta, J.L. Mattei, P. Queffelec, Ceram. Int. 42 (2016) 8413–8418.
[17] A.V. Trukhanov, V.O. Turchenko, I.A. Bobrikov, S.V. Trukhanov, I.S. Kazakevich, A.M. Balagurov, J. Magn. Magn. Mater. 393 (2015) 253–259.
[18] S.V. Trukhanov, A.V. Trukhanov, V.O. Turchenko, V.G. Kostishin, L.V. Panina, I.S. Kazakevich, A.M. Balagurov, J. Magn. Magn. Mater. 417 (2016) 130–136.
[19] S.V. Trukhanov, A.V. Trukhanov, et al., J. Magn. Magn. Mater. 426 (2017) 554–562.
[20] K.M.U. Rehman, et al., J. Supercond. Novel Magn. (2017) 1–8, https://doi.org/10.1007/s10948-017-4272-5.
[21] K.M.U. Rehman, et al., Chin. J. Phys. 55 (2017) 1780–1786.
[22] S.V. Trukhanov, Investigation of stability of ordered manganites, JETP 101 (2005) 513–520.
[23] S.V. Trukhanov, A.V. Trukhanov, H. Szymczak, C.E. Botez, J. Low Temp. Phys. 149 (2007) 185–199.
[24] S.V. Trukhanov, A.V. Trukhanov, A.N. Vasil'ev, A. Maignan, H. Szymczak, JETP Lett. 85 (2007) 507–512.
[25] S.V. Trukhanov, A.V. Trukhanov, A.N. Vasiliev, H. Szymczak, JETP 111 (2010) 209–214.
[26] S.V. Trukhanov, D.P. Kozlenko, A.V. Trukhanov, J. Magn. Magn. Mater. 320 (2008) e88–e91.
[27] S.V. Trukhanov, A.V. Trukhanov, S.G. Stepin, H. Szymczak, C.E. Botez, Phys. Sol. State 50 (2008) 886–893.
[28] S.B. Galvão, A.C. Lima, S.N. deMedeiros, J.M. Soares, C.A. Paskocimas, Mater. Lett. 115 (2014) 38–41.
[29] V.A. Rane, S.S. Meena, S.P. Gokhale, S.M. Yusuf, G.J. Phatak, S.K. Date, J. Electron. Mater. 42 (2013) 761–768.
[30] Z.F. Zi, Y.P. Sun, X.B. Zhu, Z.R. Yang, J.M. dai, W.H. Song,, J. Magn. Magn. Mater. 320 (2008) 2746–2751.
[31] T.B. Ghzaiel, W. Dhaoui, A. Pasko, F. Mazaleyrat, J. Alloy. Compd. 671 (2016) 245–253.
[32] B. Grindi, Z. Beji, G. Viau, A. BenAli, J. Magn. Magn. Mater. 449 (2018) 119–126.
[33] Y. Yang, F. Wang, X. Liu, J. Shao, S. Feng, D. Huang, M. Li, J. Magn. Magn. Mater. 422 (2017) 209–215.
[34] J. Li, H.W. Zhang, Q. Li, Y.X. Li, Q.L. Yu, J. Rare Earths 31 (2013) 983–987.
[35] Y.J. Yang, X.S. Liu, D.L. Jin, Mater. Sci. Eng. B 186 (2014) 106–111.
[36] J. Park, Y.-K. Kim, S.-G. Kim, S. Kim, L.S.I. Liyanage, J. Lee, W. Lee, G.S. Abo, K.-H. Hur, S.-Y.A., J. Magn. Magn. Mater. 355 (2014) 1–6.
[37] A. Thakur, R.R. Singh, P.B. Barman, J. Magn. Magn. Mater. 326 (2013) 35–40.
[38] W.J. Zhang, Y. Bai, X. Han, L. Wang, X.F. Lu, L.J. Qiao, J.L. Cao, D. Guo, J. Alloy.

Compd. 556 (2013) 20–25.
[39] K.M.U. Rehman, X. Liu, M. Li, S. Jiang, et al., J. Magn. Magn. Mater. 426 (2017) 183–187.
[40] M. Mozaffari, A. Arab, M.H. Yousefi, J. Amighian, J. Magn. Magn. Mater. 322 (2010) 2670–2674.
[41] H.Z. Wang, Y.N. Hai, B. Yao, Y. Xu, L. Shan, L. Xu, J.L. Tang, Q.H. Wang, J. Magn. Magn. Mater. 422 (2017) 204–208.
[42] B.K. Rai, S.R. Mishra, V.V. Nguyen, J.P. Liu, J. Alloy. Compd. 550 (2013) 198–203.
[43] Long Peng, Lezhong Li, Xiaoxi Zhong, Rui Wang, Tu. Xiaoqiang, J. Magn. Magn. Mater. 411 (2016) 62–67.
[44] Y.J. Yang, X.S. Liu, Mater. Technol. 29 (2014) 232–236.
[45] I.A. Auwal, B. Ünal, H. Güngüneş, S.E. Shirsath, A. Baykal, Ceram. Int. 42 (2016) 9100–9115.
[46] W.M.S. Silva, N.S. Ferreira, J.M. Soares, R.B. daSilva, M.A. Macêdo, J. Magn. Magn. Mater. 395 (2015) 263–270.
[47] S.K. Chawla, S.S. Meena, P. Kaur, P.K. Mudsainiyan, S.M. Yusuf, J. Magn. Magn. Mater. 378 (2015) 84–91.
[48] S.K. Chawla, P.K. Mudsainiyan, S.S. Meena, S.M. Yusuf, J. Magn. Magn. Mater. 350 (2014) 23–29.
[49] C. Kittel, Introduction to Solid State Physics, Wiley, New York, 2005.
[50] Z.M. Wang, Ferrite Production Technology, Chongqing University Press, Chongqing, 2013.